

# Lawrence Berkeley National Laboratory

## Recent Work

### Title

n+-P TOTAL CROSS SECTIONS IN THE RANGE 450 Mev TO 1650 Mev

### Permalink

<https://escholarship.org/uc/item/0wc241dz>

### Author

Devlin, Thomas J.

### Publication Date

1961-03-06

UCRL 9548

Cy. 2

UNIVERSITY OF  
CALIFORNIA

*Ernest O. Lawrence*

*Radiation  
Laboratory*

BERKELEY, CALIFORNIA

## **DISCLAIMER**

This document was prepared as an account of work sponsored by the United States Government. While this document is believed to contain correct information, neither the United States Government nor any agency thereof, nor the Regents of the University of California, nor any of their employees, makes any warranty, express or implied, or assumes any legal responsibility for the accuracy, completeness, or usefulness of any information, apparatus, product, or process disclosed, or represents that its use would not infringe privately owned rights. Reference herein to any specific commercial product, process, or service by its trade name, trademark, manufacturer, or otherwise, does not necessarily constitute or imply its endorsement, recommendation, or favoring by the United States Government or any agency thereof, or the Regents of the University of California. The views and opinions of authors expressed herein do not necessarily state or reflect those of the United States Government or any agency thereof or the Regents of the University of California.

UCRL-9548  
Physics Distribution  
TID-4500 (16th Ed.)

UNIVERSITY OF CALIFORNIA  
Lawrence Radiation Laboratory  
Berkeley, California

Contract No. W-7405-eng-48

$\pi^{\pm}$ -p TOTAL CROSS SECTIONS IN THE RANGE  
450 Mev TO 1650 Mev  
Thomas J. Devlin  
(Ph. D. Thesis)

March 6, 1961

$\pi^{\pm}$ -p TOTAL CROSS SECTIONS IN THE RANGE  
450 Mev TO 1650 Mev

<u>Contents</u>	
Abstract . . . . .	3
I. Introduction . . . . .	4
II. Experimental Method	
A. General . . . . .	6
B. Beam Optics . . . . .	6
C. Hydrogen Target . . . . .	10
D. Counters . . . . .	10
E. Gas Cerenkov Counter and Pressure Curves . . . . .	14
F. Liquid Nitrogen Cerenkov Counter . . . . .	16
G. Electronics . . . . .	18
III. Analysis of Data	
A. General . . . . .	20
B. Energy Corrections . . . . .	21
C. Accidentals Corrections . . . . .	21
D. Coulomb Scattering Correction . . . . .	25
E. Muon and Electron Contamination . . . . .	28
F. Extrapolation to Zero Solid Angle . . . . .	32
G. Proton Contamination . . . . .	35
IV. Results . . . . .	38
V. Discussion	
A. General . . . . .	43
B. Cross Section for Pure T = 1/2 State . . . . .	43
C. Resonant States . . . . .	44
D. Application of Dispersion Relations . . . . .	48
E. Comparison Between Scattering and Photoproduction . . . . .	49
Acknowledgments . . . . .	52
Appendices	
A. Derivation of Method for Coulomb Scattering Correction . . . . .	53
B. Partial-Wave Analysis . . . . .	55
References . . . . .	58

$\pi^{\pm}$ -p TOTAL CROSS SECTIONS IN THE RANGE  
450 Mev TO 1650 Mev

Thomas J. Devlin

Lawrence Radiation Laboratory  
University of California  
Berkeley, California

March 6, 1961

ABSTRACT

The total scattering cross sections for positive and negative pions on hydrogen was measured at frequent intervals in the energy range from 450 Mev to 1650 Mev. Six scintillation counters measured the transmission of pions at various solid angles, and the results were extrapolated to zero solid angle. Two peaks previously discovered in the  $\pi^{-}$ -p cross section were measured and found to be centered at  $600 \pm 15$  Mev and  $900 \pm 15$  Mev. A broad maximum was observed in the  $\pi^{+}$ -p cross section at approximately 1350 Mev. A "shoulder" at approximately 800 Mev, in a region where the  $\pi^{+}$ -p cross section is rapidly rising, gives some support to speculation that there is a resonant state at this energy.

## I. INTRODUCTION

Prior to 1955, little work was done in the investigation of pion-proton scattering above 300 Mev.<sup>1</sup> Since that time, several experiments have indicated that there is a great deal of structure in the graph of total cross section vs energy from 300 Mev to 2 Bev. Investigations at the Brookhaven Cosmotron<sup>2</sup> indicated the presence of broad maxima in the  $\pi^-$ -p cross section at 900 Mev, and in the  $\pi^+$ -p cross section at 1.4 Bev. A group from MIT working at the Bevatron resolved the broad maximum in the  $\pi^-$ -p cross section into two peaks.<sup>3</sup> The energies at which these peaks occurred were somewhat higher than those indicated by the corresponding peaks in the pion photoproduction cross section.<sup>4</sup> Recent work, including that presented here, has resolved this discrepancy.\*

The purpose of the experiment described here was to investigate in detail the behavior of the pion-proton total cross section as a function of energy from 450 Mev to 1650 Mev. The following criteria were used in designing the experiment:

1. Accurate determination of kinetic energy (1 to 2%);
2. Good statistical accuracy (2%);
3. Measurement of  $\pi^+$ -p and  $\pi^-$ -p cross sections under the same experimental conditions for use in dispersion relations, and for determination of cross section for the isotopic spin ( $T = 1/2$ ) state;
4. Accurate determination of beam contamination by particles other than pions, the effect of Coulomb scattering, and other spurious effects; and
5. Provision of some information about the quantum numbers involved if the peaks are, in fact, due to resonant states.

---

\* A group working at Saclay has measured the total cross section over much of the energy range covered here with essentially the same results.<sup>21</sup>

No formal theory yet exists allowing a calculation of the expected pion-proton cross section in this energy range; however, the results of experiments can yield some qualitative information about the nature of the interaction.<sup>4</sup>

## II. EXPERIMENTAL METHOD

### A. General

The general method for measuring the cross sections was that for a transmission experiment. The attenuation of pions by hydrogen was measured by comparing the difference in attenuation by a full and an empty liquid hydrogen target. This method automatically corrects for such spurious effects as counter inefficiency and attenuation by target walls and other material in the beam.

Pions were produced by collision of the internal circulating proton beam of the Bevatron with a 1-1/2-in. platinum target. The pions thus produced were brought to the hydrogen target by a magnetic optical system, and were monitored by a series of scintillation counters. The experimental arrangement is shown in Fig. 1.

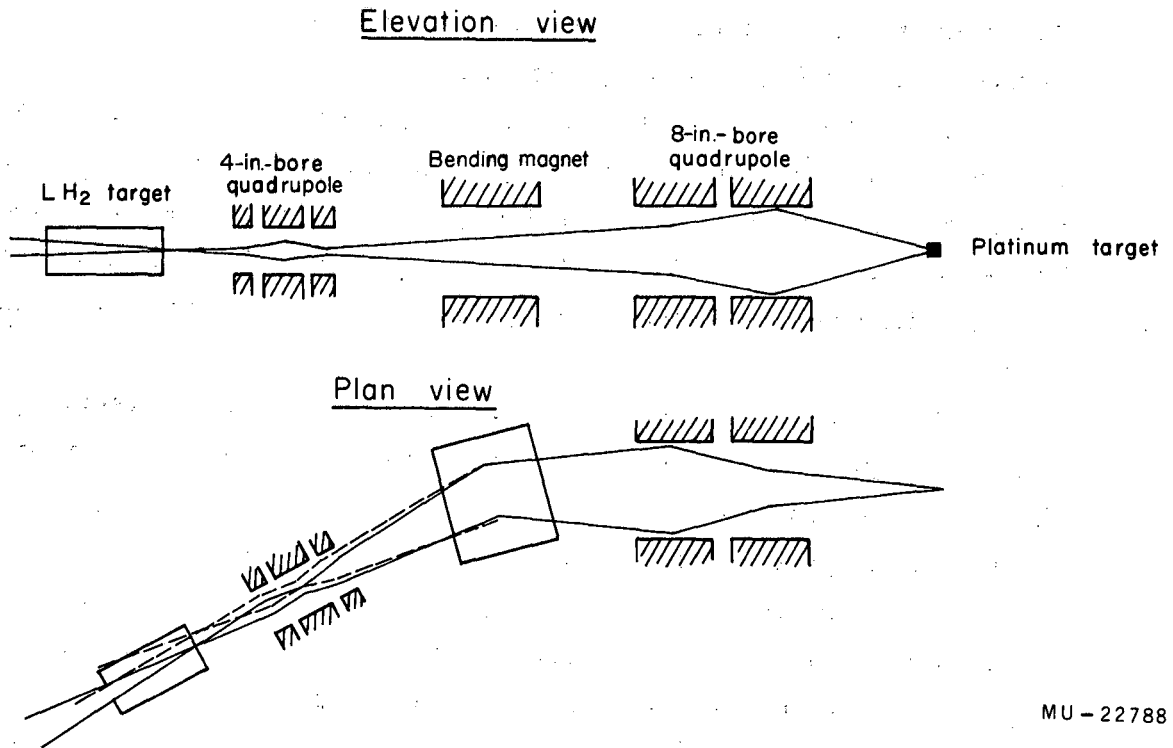
### B. Beam Optics

The optical system is shown schematically (not to scale) in Fig. 2: It consists of an 8-in. -bore focusing quadrupole doublet with two 32-in. -long sections, an 18x36-in. H-type bending magnet, and a 4-in. -bore focusing quadrupole triplet with sections 8 in., 16 in., and 8 in. long. We refer to these below as  $Q_1$ , B, and  $Q_2$  respectively.

Pions emitted from the platinum target at 36.5 deg from the forward direction of the circulating proton beam were collected by  $Q_1$ . The effective aperture of  $Q_1$  subtended a solid angle of approximately 2 milliradians from the platinum target.

$Q_1$  was operated in a manner designed to bring the beam to a focus at the final transmission counter  $M_3$ . This was complicated somewhat by the focusing action of the bending magnet. The orientation of the bending magnet was such that the angles which the beam center line made with respect to the entrance and exit faces of the magnet were equal. With this orientation, there is no focusing action in the horizontal plane. However, there is a focusing action in the vertical plane. Since the focal lengths of the quadrupole in the two planes can be varied independently by proper adjustment of the currents in the





MU - 22788

Fig. 2. Diagram of beam optics (not to scale).

two field sections, it was possible to compensate for the effect of the bending magnet by proper setting of the quadrupole currents. Considered by itself, the quadrupole produced an astigmatic focus, i. e., the image distances were different in the horizontal and vertical planes. However, the combination of quadrupole and bending magnet produced an anastigmatic focus at the position of  $M_3$ .

$Q_2$  acted as a field lens. Its purpose was to optimize the flux of particles through  $M_3$  and the hydrogen target. Since  $Q_2$  was not placed exactly at the position of the optical image, it was necessary to further adjust the currents in  $Q_1$  in order to maintain the image at  $M_3$ .  $Q_2$  increased the flux through  $M_3$  by approximately a factor of two.

The momentum analysis of the beam was accomplished by the bending magnet, B. The angle of bend was 23.28 deg. The monochromatic beam incident on Counter  $M_3$  had a width in energy at half maximum of approximately 1-1/2%.

The currents for the quadrupoles were determined before the experiment by use of an analogue computer capable of generating a curve corresponding to the path of a charged particle through regions of a given magnetic field gradient. These values were later checked by use of the floating-wire technique. During the experiment, the current values were adjusted slightly in order to optimize the flux of particles through the counter system.

Since the determination of the kinetic energy or momentum of the beam was of great importance, great care was exercised in measuring the current in the bending magnet necessary to produce a particle of given momentum in the system. The curve of momentum vs magnet current was measured four times while the magnet was in place. All measurements agreed to approximately 1%.

The pressure curves taken with the gas Cerenkov counter described below were consistent with the wire-orbit measurements on the magnet. The threshold pressure for counting pions occurred at the point expected from the magnet measurements.

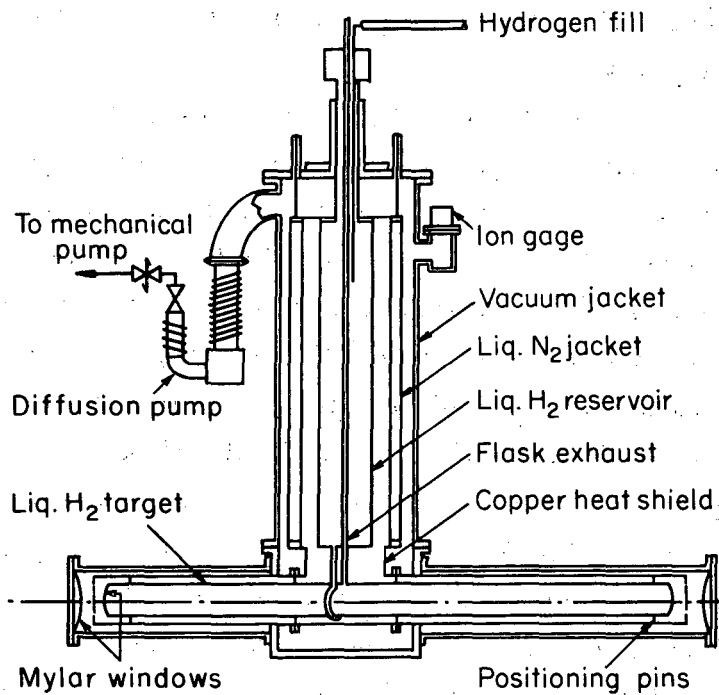
### C. Hydrogen Target

The liquid hydrogen target is shown in Fig. 3, and is described in detail in Ref. 5. The target was designed specifically for transmission experiments using high-energy particles. Since the density of liquid hydrogen is so low, 0.071 g/cc, the target was made quite long, 48 in., in order to obtain a reasonable attenuation of the beam, and thus good statistical accuracy.

The target consists of a hydrogen reservoir surrounded by a liquid nitrogen jacket, which is in turn surrounded by the outside steel jacket of the vacuum container. Below the hydrogen reservoir and connected to it is a 4-ft-long hydrogen flask surrounded by a concentric copper tube maintained at liquid nitrogen temperature by thermal contact with the liquid nitrogen reservoir. The hydrogen flask is made of 4-in. (o. d.) stainless steel tubing with 1/32-in. walls. The end windows of the flask are made of two sheets of 0.010-in. -thick Mylar cemented together with an epoxy resin mixture. The outer windows are made of 0.030-in. -thick Mylar. The exact length of the hydrogen flask is 48-7/8 in. measured from the centers of the Mylar windows at a pressure difference of 1 atm. The large diameter of the flask (4 in.) prevented any of the particles counted by the final 1-1/2-in. -diameter scintillation counter from illuminating the target walls.

### D. Counters

All the counters, except the Cerenkov counters, were plastic scintillation counters made of a solid solution of terphenyl in polystyrene. The sizes of the counters are listed in Table I. All the scintillators were viewed through lucite light pipes by RCA 6810A photomultiplier tubes. High-capacitance tube bases were used for all counters because of the high singles counting rates expected in counters exposed to the main pion beam.



MU-18521

Fig. 3. Liquid hydrogen target.

Table I

Counter geometries					
Counter	Diameter (inches)	Thickness (inches)	Solid angle for counter positions (milliradians)		
			I	II	III
M <sub>1</sub>	2.00	0.25	-	-	-
M <sub>2</sub>	4.00	0.50	-	-	-
M <sub>3</sub>	1.50	0.25	-	-	-
S <sub>0</sub>	8.00	0.50	-	-	-
S <sub>1</sub>	10.60	0.50	7.13	7.13	-
S <sub>2</sub>	11.00	0.50	7.03	6.868	7.00
S <sub>3</sub>	12.00	0.50	4.88	5.606	6.00
S <sub>4</sub>	12.00	0.50	3.76	4.344	5.00
S <sub>5</sub>	12.00	0.50	2.64	3.082	4.00
S <sub>6</sub>	12.00	0.50	1.52	1.82	3.00

Counters  $M_1$  and  $M_3$  determined the geometry of the pion beam incident on the hydrogen target. Their sizes represent a compromise between the necessity to obtain a high counting rate for good statistical accuracy, and of keeping the divergence of the beam low in order to prevent a large Coulomb scattering effect and illumination of the target walls.

Counter  $M_2$  did not define the geometry of the beam. Its purpose was to reduce the number of accidental counts in the monitor system.

$S_0$  was placed close to and immediately following the hydrogen target in such a way that all particles that struck the transmission counters had to pass through  $S_0$  first. The large area of the transmission counters necessitated the use of  $S_0$ . Its purpose was to provide a triple coincidence with the output of the monitor coincidence circuit and each of the transmission counters, thus reducing the accidental counting rate.

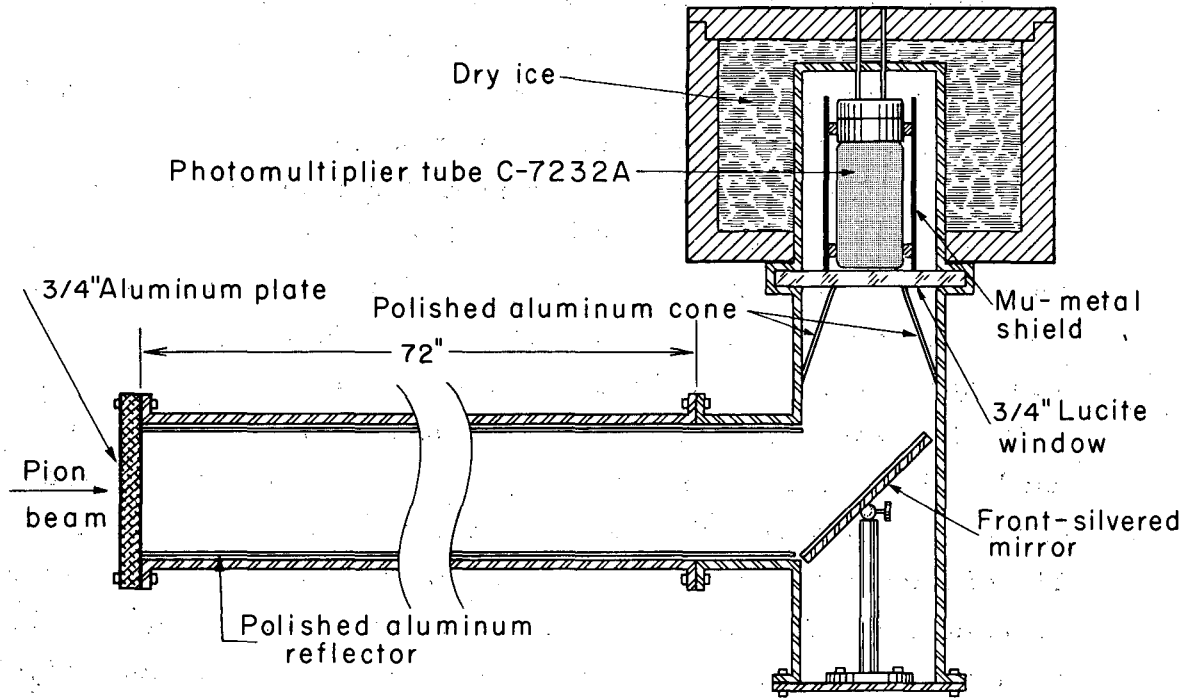
The transmission counters  $S_1$  through  $S_6$  subtended various solid angles from the center of the hydrogen target.  $S_1$  was kept at 7 msr throughout the experiment.  $S_6$ , which subtended the smallest solid angle, was moved several times. At the higher energies it subtended about 1.5 msr and, at lower energies, 3 msr. The change was made because the greater amount of Coulomb scattering at lower energies in the smaller solid angles made the data somewhat dubious. The other counters were moved also in order to maintain equal intervals of solid angle from  $S_1$  to  $S_6$ . The three sets of solid angles used are listed in Table I. The use of cross sections measured at various angles to extrapolate to perfect geometry is discussed in Sec. III F.

### E. Gas Cerenkov Counter and Pressure Curves

The gas Cerenkov counter shown in Fig. 4 is described in detail in Ref. 6. It served a twofold purpose in the experiment: (a) to continuously reject protons in the positive beams, and (b) to determine, by means of pressure curves, the number of protons, muons, and electrons contaminating the pion beams.

The effective volume of the gas counter was 7 ft long and 4 in. in diameter. It was filled with sulfur hexafluoride as the radiating material. The pion beam was attenuated by about 35% because of scattering in this counter. When used in the monitor to reject protons, the counter was kept at a pressure of 230 psig, corresponding to a threshold velocity for Cerenkov radiation of 0.985 c. This pressure was adequate for counting pions with a kinetic energy above 675 Mev. Below this energy, a liquid nitrogen counter, described below, was used. Throughout the energy range of the experiment, the velocities of the protons were well below the threshold velocity of the gas counter. The efficiency of the gas counter for counting pions was measured to be about 95%. This was determined on negative beam by calculating the ratio of coincidences between the Cerenkov counter and  $M_2M_3C$ , to coincidences in  $M_2M_3$  alone.

No adequate method was found for measuring the efficiency of the gas counter for counting protons. It was assumed to be zero. The possibility that delta rays produced in the counter by protons would give enough Cerenkov light to be counted was investigated. It was calculated that an appreciable number of protons (about 10% at the highest energies encountered in the experiment) produced  $\delta$  rays with velocities above the Cerenkov threshold. However, the energy of the  $\delta$  rays thus produced was just barely above the threshold, and the amount of light collected by the phototube was insufficient to produce a signal of any appreciable size.



MU-16403

Fig. 4. Gas Cerenkov Counter.

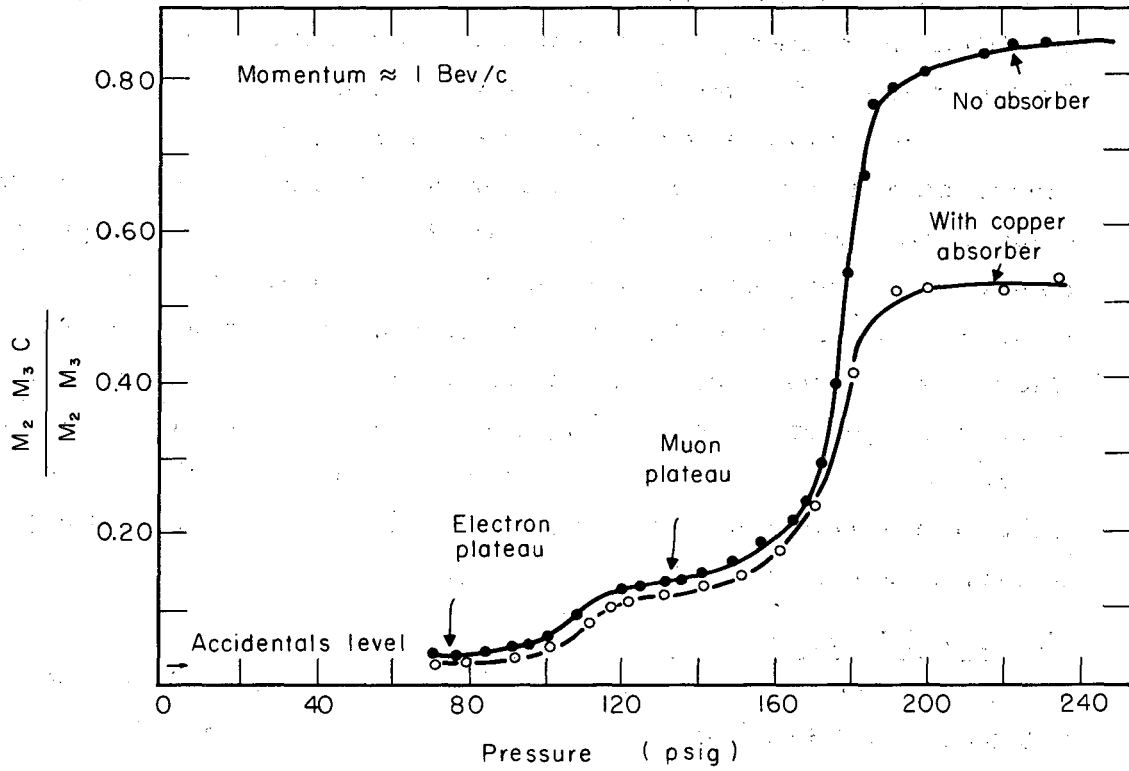
Although the Cerenkov counter itself was probably 100% efficient in rejecting protons, the total monitoring system was only 93% to 98% efficient for proton rejection. The lowered efficiency was due to accidental coincidences between protons passing through the scintillation counters, and a spurious count in the Cerenkov counter. This is discussed in more detail in Sec. III-G.

The contamination of muons and electrons in the beam was measured by the pressure-curve method. The response of the Cerenkov counter was determined as a function of the pressure of the gas in the counter. As the pressure was varied, the temperature was observed in order to ensure that it remained constant at room temperature. The index of refraction of the gas is given as a function of pressure at room temperature in Ref. 6. One of the curves obtained is shown in Fig. 5. The various constituents of the beam are clearly shown. These measurements, including the function of the copper mentioned in Fig. 5, are discussed in Sec. III-E.

#### F. Liquid Nitrogen Cerenkov Counter

For measurements of the  $\pi^+$  cross section from 450 Mev to 675 Mev, a liquid nitrogen Cerenkov counter was substituted for the gas Cerenkov counter. The index of refraction of liquid nitrogen ( $n = 1.2053$  at its boiling point) was adequate to separate pions from protons in this energy range.

The counter was constructed quite simply by putting a 6810A phototube with a lighttight seal on the neck of a nitrogen Dewar. The phototube was easily removed for checking the level of nitrogen and filling the Dewar. Although the nitrogen level was kept low enough so that it never came in physical contact with the phototube, the tube was maintained at a very low temperature. This had the desirable effect of a low noise level in its output. Qualitative checks on the counter showed it to be nearly 100% efficient. Since any inefficiency would have no effect on the cross section, no attempt was made to determine it exactly.



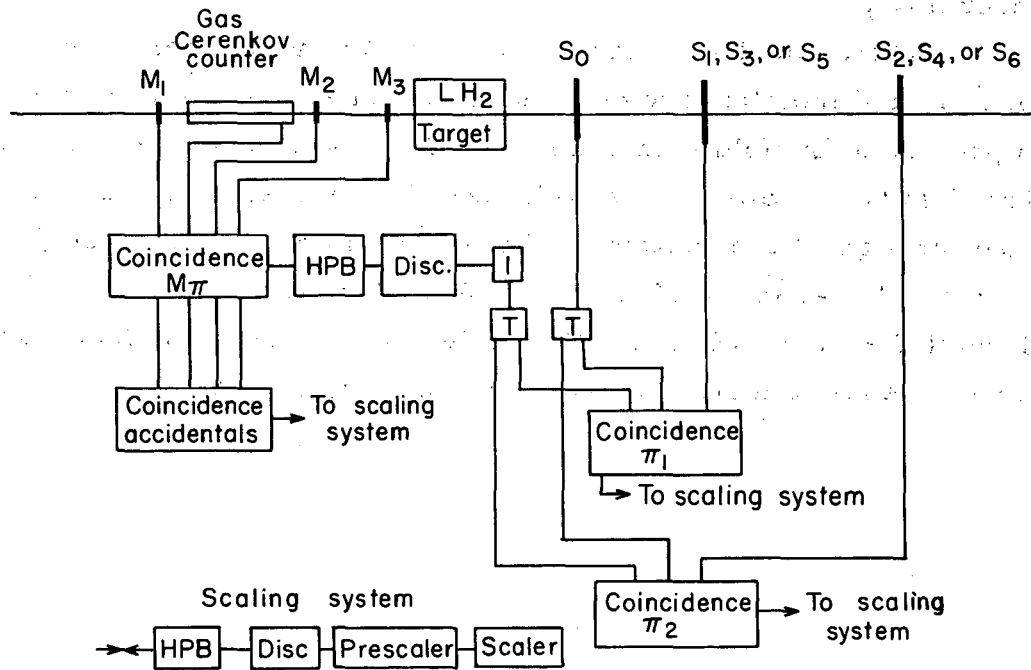
MU-22791

Fig. 5. Gas Cerenkov counter pressure curves.

G. Electronics

The electronics system for this experiment is shown in Fig. 6. The setup was exactly the same for both positive and negative beam except that the Cerenkov counter was physically removed from the negative beam, and the monitor coincidence circuit was changed accordingly.

The coincidence circuits were all of the Wenzel type.<sup>7</sup> The monitor and monitor-accidentals coincidence circuits were modified to provide a fourfold coincidence. All the others were of the standard threefold type. Swift-Perez-Mendez discriminator-amplifiers were used throughout the system.<sup>8</sup> The distributed amplifiers employed were Hewlett-Packard 460A and 460B. The prescalers were Hewlett-Packard 520A, and the scalers are of the type described in the Lawrence Radiation Laboratory Counting Handbook.<sup>9</sup>



MU - 22855

Fig. 6. Block diagram of electronics. Not all coincidences are shown. Signals from  $M_\pi$  and  $S_0$  are continued through coincidence,  $\pi_1$ , into another coincidence with counter,  $S_3$ , and subsequently with  $S_5$  and the beam distribution counter. Similarly, coincidence,  $\pi_2$ , begins another chain of coincidence circuits yielding information on counters  $S_4$ ,  $S_6$ , and finally, an accidentals measurement.

### III. ANALYSIS OF DATA

#### A. General

The basic technique of the transmission experiment involves a comparison of the attenuation of a beam of particles with the scattering material present and absent. In terms of the intensity of a particle beam, we have

$$I = I_0 e^{-n\sigma x},$$

where  $I_0$  is the intensity of particles incident on an attenuating material  $x$  cm long, with a density of  $n$  scattering centers per  $\text{cm}^3$ , and a total attenuation cross section of  $\sigma \text{ cm}^2$ .  $I$  is the intensity of the beam after attenuation by the material. In any experimental setup, there are materials in the beam other than the material under investigation. These contribute an "empty-target effect." If we let  $I = I_e$  be a measurement of transmitted intensity when the target is empty, and  $I = I_f$  be the same measurement with a full target, then

$$\sigma = \frac{1}{nx} \ln \frac{I_e}{I_f},$$

where  $n$ ,  $x$ , and  $\sigma$  refer only to the liquid hydrogen.

In this experiment,  $I_e$  and  $I_f$  were given by the ratios of transmission coincidences to monitor coincidences,

$$I = M_1^i M_2 M_3 C S_0 S_i / M_1 M_2 M_3 C,$$

where  $i$  refers to any one of the transmission counters,  $S_1^i$  to  $S_6$ .

In this way, a cross section was calculated for each of the transmission counters. The results were corrected for accidentals, muon and electron contamination, and Coulomb scattering. Then the resulting cross sections, as functions of solid angle, were extrapolated to zero solid angle. In the case of the  $\pi^+$ -p cross sections, a further correction was applied for contamination of the beam by protons. These corrections are described in detail below.

### B. Energy Corrections

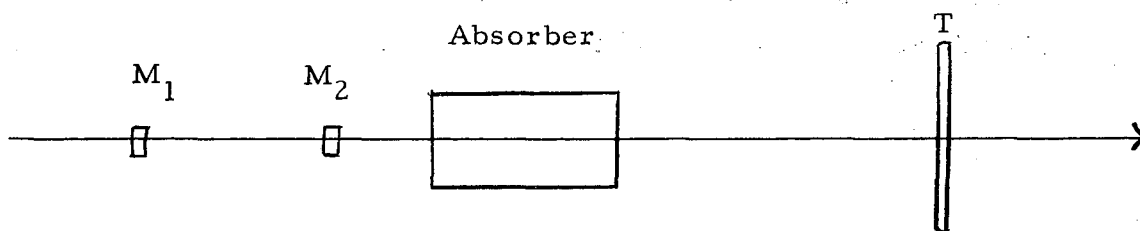
It was necessary to correct the energy determined by the bending magnet because of energy loss in air, counters, target walls, and the hydrogen itself. This was done in a standard manner, using range and  $dE/dx$  tables.<sup>10</sup> The correction amounted to about 25 Mev in the  $\pi^-$  beam and about 80 Mev in the  $\pi^+$  beam. The difference is due to the presence of the Cerenkov counter in the positive beam.

Although the accuracy of the energy measurement was about 1-1/2%, the energy spread, i. e., the band of energies involved in any one cross-section measurement, was about  $\pm 20$  Mev from the central energy. This was because the hydrogen target was so long. Therefore all cross sections measured in this experiment represent an average over 40 Mev in energy. It is to be expected that this has little effect on the results in regions where the slope of cross section versus energy is relatively constant, but one must examine the effect at peaks and valleys in the cross section where the slope is rapidly changing. The effect of averaging over a band of energies was investigated in some detail in the region of the peaks in the cross section and was found to be negligible (of the order of 0.2 millibarn, with an uncertainty about the same).

### C. Accidentals Corrections

Most types of accidental counts have only a small effect on the results of a transmission experiment. However, there is one type which changes the value of the apparent cross section by a percentage approximately equal to the percentage of accidental counts. We will discuss this type of accidental in some detail.

Assume a monitor telescope, absorber, and transmission counter system as pictured below:



Assume that the monitor counters are small compared with the size of the absorber and transmission counters and also that the cross section of the beam is larger in area than the area of the monitor counters. The mathematical arguments involved are independent of these assumptions, but these are the conditions under which the experiment was performed.

The type of accidental to be considered is that in which a true beam particle--i. e., one that passes through the monitor counters-- is scattered out of the transmission counter, but because of a spurious count in the transmission counter, appears to be unscattered. The spurious count may be caused by another true beam particle which comes through the monitor, or by a beam particle which misses the monitor but still hits the transmission counter, or by general background in the area of the transmission counter, all within the resolving time of the electronics.

The important point of this type of accidental is that it discriminates between scattered particles and unscattered particles. That is, it has no effect whatsoever on those particles not scattered out of the transmission counter, but causes some of the scattered particles to appear to be unscattered. Therefore, we must weight the effect of accidentals by the probability that the particle is scattered. We develop this effect mathematically below, where

$$P = (\text{No. of real counts, } M_1 M_2 T) / (\text{No. of real counts, } M_1 M_2),$$

$$A = (\text{No. of accidental counts } M_1 M_2 T) / (\text{No. of real counts, } M_1 M_2),$$

Subscripts E and F, refer to target empty or full,

$(1 - P)$  = Probability that a particle is scattered out of T, and

$(1 - P_E)$  = Probability that a particle is scattered by the empty target; should be small.

The number of scattered particles per monitor count replaced by accidental counts in the transmission counter is  $A(1 - P)$ .

The true cross section is given by

$$\sigma_t = \frac{1}{nx} \ln \frac{P_E}{P_F}$$

and the error in the cross section is

$$\Delta\sigma = \frac{1}{nx} \left( \frac{\Delta P_E}{P_E} - \frac{\Delta P_F}{P_F} \right)$$

The measured cross section, uncorrected for accidentals, is

$$\sigma_m = \frac{1}{nx} \ln \left( \frac{P_E + A_E (1 - P_E)}{P_F + A_F (1 - P_F)} \right) = \frac{1}{nx} \ln \frac{P_E + \Delta P_E}{P_F + \Delta P_F}$$

We now make assumptions about the variation of  $A$  with target full or empty. The true behavior almost certainly lies between the following two extremes:

(a)  $A_E = A_F$ . That is, the accidentals are due mostly to counts in  $T$  that are unaffected by the target, i. e., nonbeam particles.

(b)  $A_F/A_E = P_F/P_E$ . That is, the accidentals are due mostly to particles that pass through the hydrogen target and are attenuated in the same way as those particles which pass through  $M_1$  and  $M_2$ . If we assume  $\ln \frac{P_E}{P_F} \approx \frac{P_E}{P_F} - 1$ , since  $P_E$  is only slightly greater than  $P_F$ , then we find:

$$\text{In case (a), } \frac{\Delta\sigma}{\sigma} = - \frac{A_F}{P_E}$$

$$\text{In case (b), } \frac{\Delta\sigma}{\sigma} = - A_F$$

Since  $P_E$  is close to unity, the effect on an individual transmission counter should be about the same in both cases. However, when the effect on a set of transmission counters is examined, the two cases can be quite different.

In case (a),  $A$  is dependent on the area and volume of the transmission counter, and independent of the solid angle subtended at the hydrogen target. Thus, in this experiment, since all the transmission counters were approximately the same area, the slope of the

line in a graph of apparent cross section vs solid angle is the true slope determined by the differential cross section. All the points on the graph, and the extrapolated cross section, are in error by an amount determined by the accidentals rate  $A$  and the target-empty effect,  $P_E$ .

In case (b)  $A$  depends on the focal properties of the beam. In particular, if there is a focus at the hydrogen target,  $A$  is proportional to the solid angle subtended by the counter, and tends to extrapolate to a negligible effect as the cross section is extrapolated to zero solid angle.

During the experiment only one coincidence circuit was available for this type of accidentals measurement. Therefore, in any given cross section measurement, there is information on the accidentals rate of only one of the transmission counters. The rates observed varied, but remained about 1% to 3%. One very definite quantitative effect observed was that the accidentals counts were attenuated in the same manner as the real counts, corresponding to case (b). Qualitatively, the rates tended to be less for smaller solid angles, but information is not complete enough to determine the exact behavior as a function of solid angle, because of differing conditions involved in the measurements under comparison.

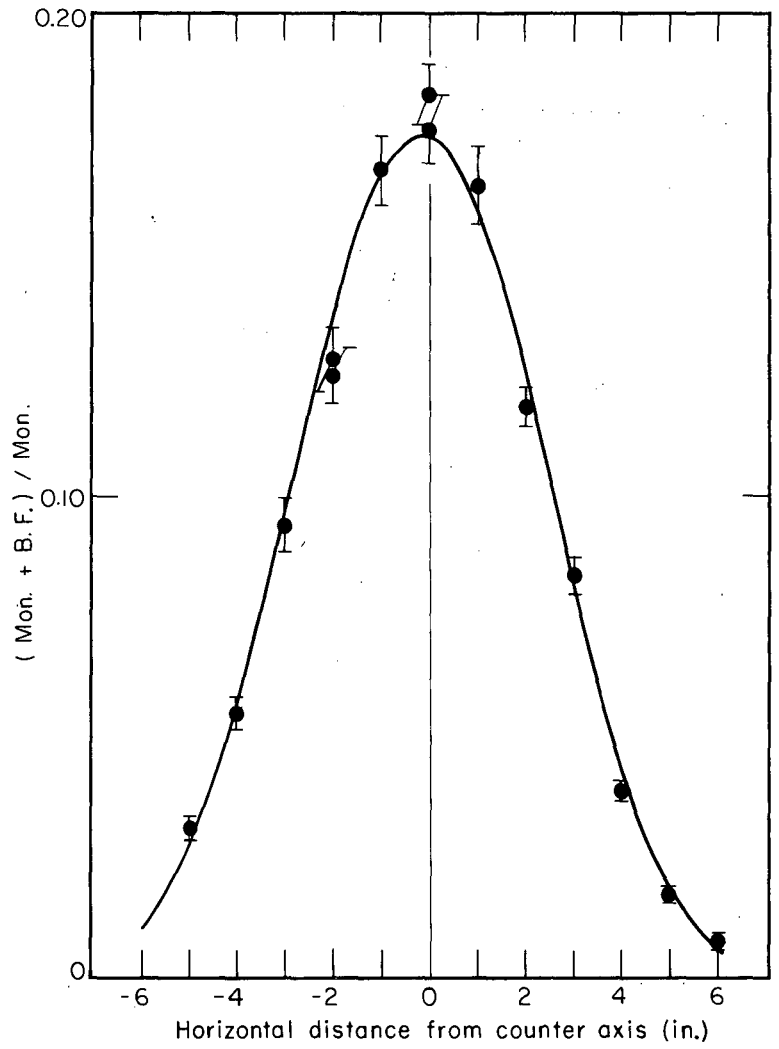
Because of the lack of information and indications that case (b) probably corresponds to the real situation involved in this experiment, no attempt was made to correct the cross section explicitly for this species of accidental, since the extrapolation to zero solid angle tends to correct automatically for this effect. Support is given to this view by the fact that the observed slopes in the extrapolation were, in general, smaller in absolute value for  $\pi^-$  than for  $\pi^+$ . This is to be expected from the lower counting rates and accidentals rates encountered in the  $\pi^-$  measurements.

#### D. Coulomb Scattering Correction

Because of the length of the hydrogen target, the measurement of the total cross section was affected appreciably by Coulomb scattering at the lower momenta and smaller solid angles. Coulomb scattering in the target walls, counters, etc., was automatically corrected for by the target-empty effect, so that only the hydrogen itself was considered in the correction.

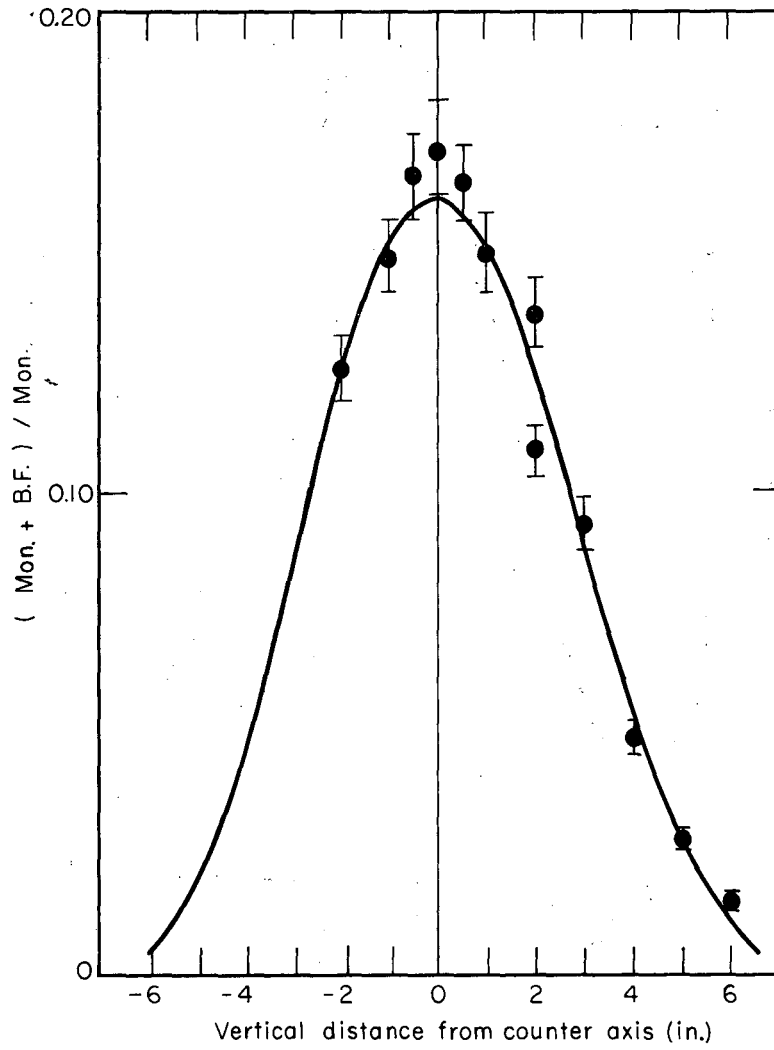
Except for the value of the mean scattering angle, the method used was essentially that of Sternheimer<sup>11</sup> (see Appendix A). The mean scattering angle quoted by Sternheimer was found to yield a correction that was obviously too large. In several measurements taken early in the experiment, before optimum beam tuning had been attained, the Coulomb scattering effect on the counter with smallest solid angle was extremely large, of the order of 10 millibarns. These cases were selected for revision of the value of the mean scattering angle. The results indicated that Sternheimer's value, revised by a factor of 0.69, gives consistent sets of corrections. This factor is somewhat smaller than that indicated by Molière theory.<sup>12</sup>

In order to employ the Sternheimer method, the flux of particles at the transmission counter must be known as a function of position over the face of the counter. This was measured by a "beam distribution counter" consisting of a small scintillation counter and long thin light pipe mounted on a frame which was movable horizontally and vertically transverse to the beam direction. Beam distributions (Figs. 7 and 8) were measured before and after the bank of transmission counters, and the results were interpolated to the positions of the individual counters. Distribution measurements were taken concurrently with almost every measurement of cross section. The corrections to those few cross sections which lacked a beam-distribution measurement were inferred from corrections calculated under similar experimental conditions.



MU-22790

Fig. 7. Horizontal Beam Distribution.



MU-22789

Fig. 8. Vertical Beam Distribution.

One set of measurements bears special mention because it gives strong support to the validity of the Coulomb correction technique which was applied. Two measurements of the  $\pi^-$  cross section at a kinetic energy of 652 Mev were taken under exactly the same conditions except for the 4-in. quadrupole tuning. The difference in the quadrupole tuning caused the beam distributions in the two cases to differ. The uncorrected cross sections differed by about 3.5 mb but, after the Coulomb correction had been applied, they differed by only 0.3 mb, well within the statistical error.

#### E. Muon and Electron Contamination

Contamination of the beam by muons is divided into two separate contributions: pion decays before and after the bending magnet. The contribution from decays after the magnet was determined by calculation alone, since the method is quite straightforward. The calculation of the contribution from decays before the magnet is much more difficult, but the pressure curves for gas Cerenkov counters provided a good check on the validity of the result. The agreement between measured and calculated values was excellent, and the calculated values were used for correcting the data.

Since the bending magnet is a momentum-selecting device, all the muons produced before the magnet and deflected into the counter telescope have the same momentum as the accepted pions. This enables us to separate the two particles by the difference in their velocities. This was done with the gas Cerenkov counter. The threshold velocity of the counter was varied by adjusting the gas pressure. Starting at high pressure, all the pions, muons, and electrons were counted. Lowering the pressure successively eliminated pions and then muons (Fig. 5). Comparison of the relative heights of the electron, muon, and pion plateaus gives the percentage of contamination of muons and electrons from contributions before the bending magnet. Muons produced after the magnet have a wide spectrum of momenta, and are not measured by this method.

In order to check on whether the second plateau was really muons, an amount of copper corresponding to one pion nuclear mean free path was inserted in front of the third telescope scintillation counter. It was expected that essentially all the muons should get through, since Coulomb scattering losses at these energies should be negligible. The strongly interacting pions should be substantially attenuated. The measurements, shown in Fig. 5, verify this.

The pressure curves were repeated at several energies, giving a measure of the contamination as a function of energy.

This contribution is fairly difficult to calculate exactly, and a number of approximations were used. Before the bending magnet, pions of many different momenta are present. The magnet accepts a certain momentum spread of pions and the same momentum spread of muons. Muons of the required momentum can come from pions of the same or greater momentum, depending on the decay angle in the center-of-mass system.

For each pion energy, there is a range of angles that will contribute acceptable muons. By calculation of the solid angle subtended by this ring of acceptable angles, we can determine what fraction of these particles decaying at each energy will contribute to the contamination. The exponential-decay law was used to determine the fraction of the total pions that decaying in each interval of path length. This was combined with the results from the acceptable solid angles, and summed over the path of the beam up to the bending magnet.

This calculation is complicated by the presence of the quadrupole focusing magnet, and approximations were necessary to handle this effect. The thin-lens equation was assumed to hold true for the quadrupole. All decays outside the focal length were assumed to contribute to the contamination. All decays between the focal point and the center of the magnet were assumed to be defocused, and were eliminated entirely from the summation. Neither of these assumptions is strictly true, but deviations from them tend to compensate for each other.

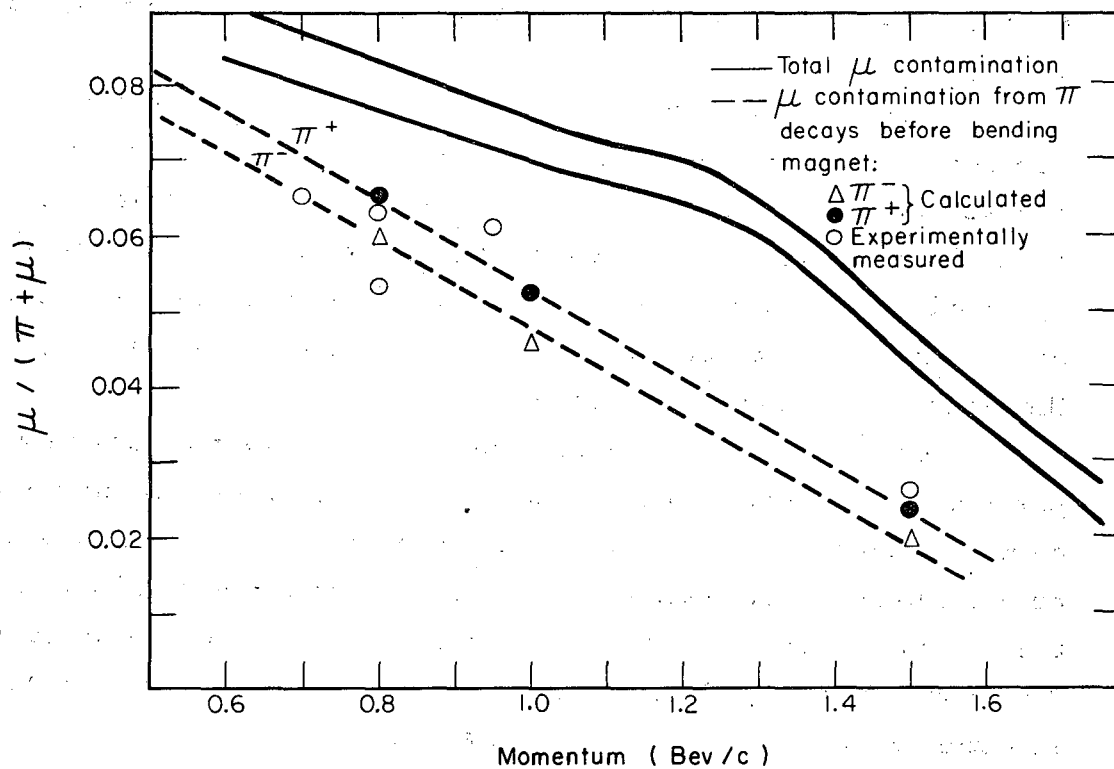
The number of pions in the beam before the bending magnet varied with energy. The counting rates observed at different energies during the experiment determined the relative number of pions of each energy, and thus the relative contribution of muons from pions of each energy.

If we take, as a function of momentum, the product of the number of pions present, the fraction decaying, and the fraction of decays in the acceptable solid angle, and plot the result vs momentum, the area under the curve is essentially the total number of muons accepted by the optical system. Dividing this by the number of pions of acceptable momentum, corrected for depletion by decays, gives the fraction of muons in the beam.

After the bending magnet, pions of only one momentum were present. These decayed into muons of equal or lesser momentum, depending on the decay angle. The criterion for determining whether or not a muon contributes to the contamination is the solid angle subtended at the point of decay by the various counters in the system. The momentum is no longer important, since there is no momentum-selection device after the bending magnet.

The calculation is straightforward, and no approximations are necessary except for summing over discrete, finite intervals of path length, rather than integrating the contribution. No experimental check was available on this contribution, but the simplicity of the calculation makes it unlikely that it is in error. The final results for muon contamination are shown in Fig. 9.

At the higher energies contamination of the beam by electrons was very small, of the order of 1%, found by comparing the relative counting rates with various quantities of lead inserted into the path of the beam, and by examining the pressure curves in the region where only electrons could count. The counting rates on the electron plateau were just slightly higher than the background rate of accidentals, and were, for this reason, rather difficult to determine exactly.



MU-22792

Fig. 9. Contamination of the pion beams by muons. The dashed curves represent the contribution from decays before the bending magnet, and the plotted points refer to these curves. The solid curves represent the total muon contamination from decays both before and after the magnet. The reason for the difference between the positive and negative muon contaminations is attenuation of the positive pions in the Cerenkov counter.

At lower energies, the number of electrons in the beam was somewhat higher. Subtraction of the accidentals rates indicated that the contamination might be as high as 5% at the lowest energies.

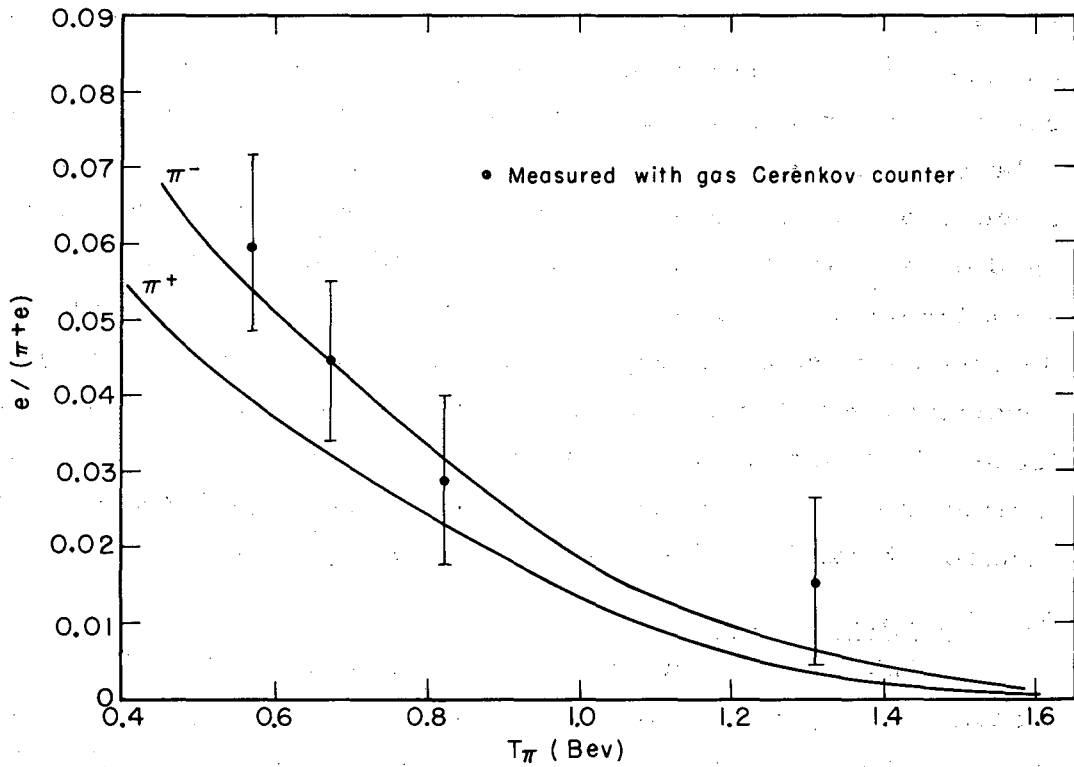
An attempt was made to calculate the amount of contamination from the spectrum of neutral pions produced in the target, the amount of platinum in the path of the gammas arising from decay of the pions, and the energy spectrum of the pair-produced electrons. Some very crude approximations were necessary in order to simplify the calculation. The results yielded contaminations roughly 50% higher than those measured by the Cerenkov counter. Although the approximations used in the calculation were probably crude enough to give invalid results for the absolute value of the contamination, it is felt that the energy dependence is substantially correct. Therefore, the calculations were renormalized to the best of the Cerenkov counter measurements, and these values were used to correct the data. The other Cerenkov counter measurements were consistent with the renormalized calculations. The electron contamination as a function of energy is shown in Fig. 10.

#### F. Extrapolation to Zero Solid Angle

Under ideal conditions, a transmission counter of finite size measures an apparent total cross section which is equal to the true total cross section diminished by an amount equal to the integral of the angular distribution of all charged particles resulting from scattering events from zero to the half-angle subtended by the counter. We may write this as

$$\sigma_M = \sigma_T - 2\pi \int_0^{\theta_1} \frac{d\sigma_{ch}}{d\Omega} \sin \theta d\theta,$$

where  $\sigma_M$  is the measured value of the cross section,  $\sigma_T$  is the true value, and  $\frac{d\sigma_{ch}}{d\Omega}$  is the value of the angular distribution for all charged particles resulting from scattering events. This angular distribution includes both the elastic angular distribution, and that for emission



MU-22793

Fig. 10. Contamination of the pion beams by electrons. The curves represent the calculated values renormalized to the measured point at 670 Mev. The difference between the values for positive and negative beams is a combination of the branching ratios for producing positive and negative pions in the platinum target, and attenuation of the positive beam by the Cerenkov counter.

of charged secondaries in the forward direction from inelastic events. The limit of integration,  $\theta_1$ , is the half-angle subtended by the transmission counter.

If several transmission counters subtending different angles are used, the graph of apparent cross section vs solid angle should lie on a line with a slope equal to the negative of the total charged differential cross section in the laboratory system, and which passes through the true value of the total cross section at zero solid angle. This is true only if the angles involved are small enough so that the differential cross section can be considered constant and equal to its value in the forward direction.

Under more realistic conditions, however, both the slope and the intercept of the line used in the extrapolation may be changed by various extraneous effects. Some of those which change the extrapolation appreciably are accidentals, Coulomb scattering, nuclear scattering in counters, etc. Of these, only the Coulomb scattering changes the intercept--i. e., the true value of the total cross section--and this correction was applied explicitly. For all the others, in those cases in which there was an appreciable effect at finite solid angles, the correction was found to extrapolate to zero with solid angle.

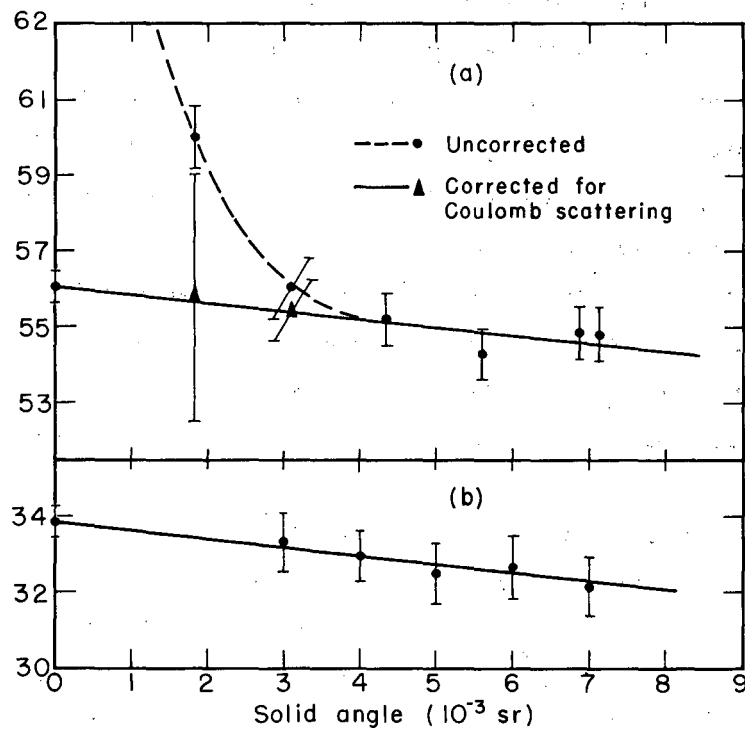
Thus we have the result that the slopes of the lines used in the extrapolation are not those indicated by the angular distributions; in fact, they are considerably larger. Because of the relatively small number of points, available for the determination of the slope (five or six), the errors involved are fairly large. However, they showed a fairly consistent tendency to remain in the range from -0.4 to -0.1 mb/msr. Because of the poor statistics involved, the slope finally employed at any given energy was the average of the slopes calculated for the surrounding energies.

Because of the small angles involved, and the small value of the slope, any uncertainty in the slope has a relatively small effect on the total cross section. The uncertainty in the slope has been included as part of the errors on the calculated values of the cross section.

Figure 11 gives examples of the extrapolation. A least-squares fit was used to calculate the slope and intercept of the lines. The slopes for all energies were then examined for consistency. In the case of the negative pions, they ranged about a value of  $-0.22$  mb/msr, with no discernible dependence on energy. For positive pions, the slopes increased with energy from about  $-0.2$  at 900 Mev to  $-0.4$  at 1600 Mev. The most likely explanation of this behavior is the production of charged secondary particles by protons contaminating the beam. Below 900 Mev the slopes get larger in absolute value, probably because of the uncertainties in the relatively large Coulomb correction applied, the Coulomb scattering of the protons in the counted beam. The energy dependence of the slopes was continued below 900 Mev and the lines used in the extrapolation were forced to fit the slopes thus determined. This fact, and the uncertainties in the Coulomb corrections in this energy range, are reflected in the relatively large errors on the points in this region.

#### G. Proton Contamination

The positively charged beam of particles was composed of approximately 75% protons and 25% pions. These percentages were determined by use of a gas Cerenkov counter. The Cerenkov counter was set at a threshold above that for counting protons and below that for counting pions. It was then put into coincidence with the scintillation counters which monitored the beam incident on the hydrogen target. Ideally, this system would count only the pions. However, this system was not 100% efficient in rejecting protons. Its efficiency for rejecting protons varied between 93% and 98%, depending on the running conditions. The only appreciable source of this inefficiency was the occurrence of an accidental count in the Cerenkov counter in coincidence with a real proton going through all the scintillation counters. This species of accidental was monitored continuously throughout the experiment. The counted beam varied between 5% and 15% protons, depending on



MU-22794

Fig. 11. Plots of apparent total cross section as a function of the solid angle subtended by the transmission counter. Curve a, taken at 895 Mev, and before optimum beam tuning shows an appreciable Coulomb scattering effect in the smaller solid angles. Curve b, taken at 1548 Mev with good beam tuning, has a negligible Coulomb effect. The line represents a two-parameter least squares fit to the corrected points. The correction for muon contamination, which is dependent on solid angle, is included in the values plotted. Electron contamination corrections and other corrections are not included, since they are not dependent on solid angle.

experimental conditions, with the rest pions and muons. These rates are consistent with an instantaneous rate of  $10^6$  background counts per second in the Cerenkov counter. Considering its position, lack of shielding, and the radio-frequency structure of the beam counting rate, this is quite a reasonable figure to expect.

Several checks verified that there really were protons in the counted beam. The simplest of these revealed that the accidentals rates on negative beam were much smaller, and quantitatively consistent with the counting rates involved.

The known proton-proton cross section and the measured percentage of protons in the counted beam were used to correct the data in an obvious manner. The correction was, in general, of the order of 1 mb or less, and tended to make the true value less than the uncorrected value.

Some ambiguity remains in relating the measured rate of accidentals to the true rate, because of the radio-frequency structure of the beam intensity. One extremely pessimistic estimate of this effect indicated a maximum change of about 15% in the correction, i. e., less than 0.15 mb change in the correction cross section. The true change necessary to compensate for the rf structure is certainly less than this. Since this correction is so small, well within the statistics on the points, no attempt has yet been made to evaluate it exactly.

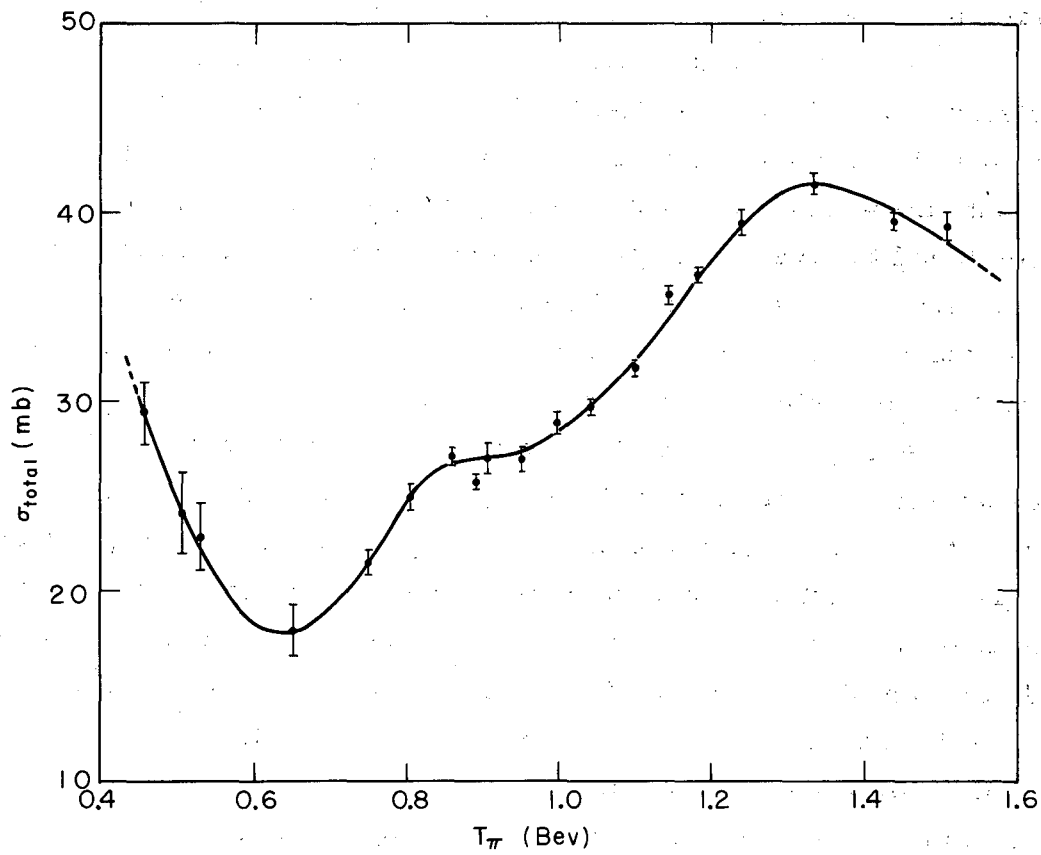
#### IV. RESULTS

The measured values of the total cross sections for  $\pi^+$ -p and  $\pi^-$ -p reactions are listed in Table II, and graphed as a function of lab pion kinetic energy in Figs. 12 and 13.

The uncertainties listed are a combination of the counting statistics, and uncertainties in the corrections applied. In several cases, the values of the cross section represent two or three measurements all within the 40-Mev energy band under study. These were combined to give a weighted average of the cross section. In two cases, the deviation of the individual points from the average was greater than one standard deviation. In these, the rms deviation was substituted for the calculated uncertainty.

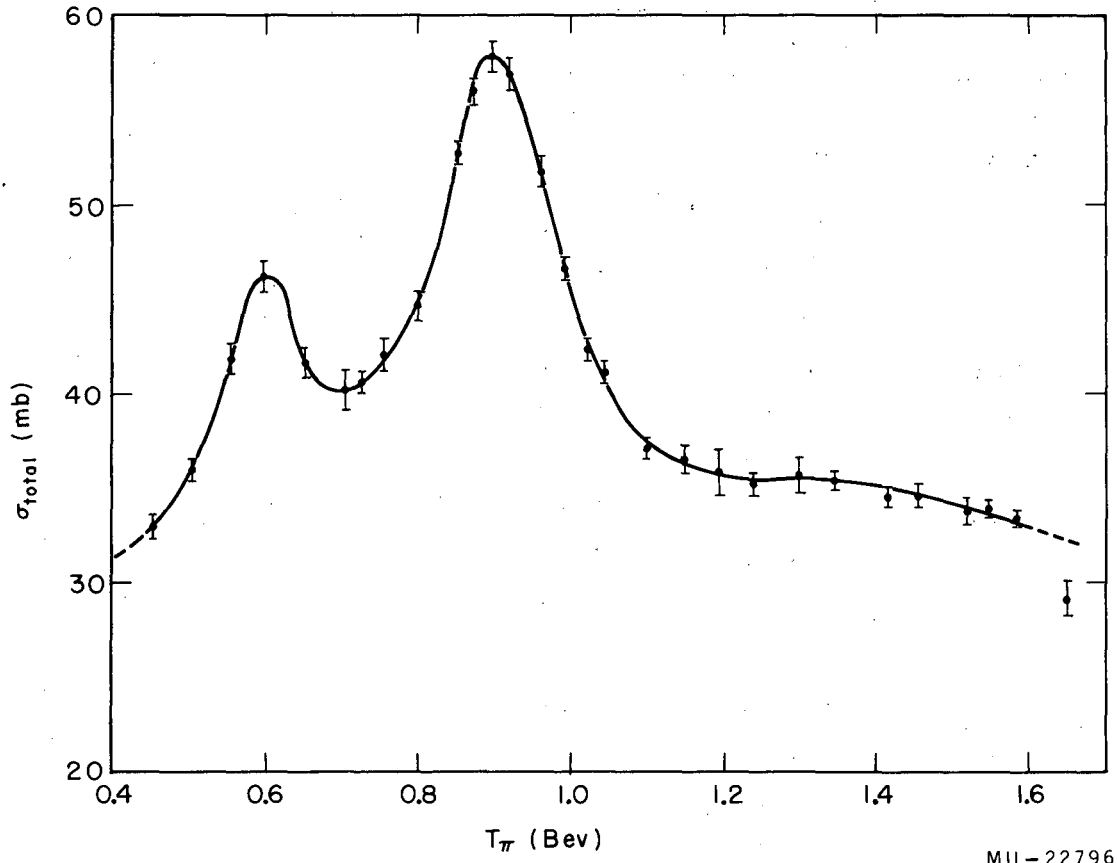
A group working at Saclay, France, has performed a similar experiment, <sup>21</sup> over part of the energy range covered in this one. Their results for the negative pion scattering are in excellent quantitative agreement with the results quoted here. Although the qualitative features of their results for positive pions are the same, there is a systematic discrepancy of about 2 to 3 mb between the two experiments, with our experiment exhibiting the higher results. The difference has not been explained, but might be ascribed to differences in the geometric correction or beam contamination. Careful re-examination of all the data and corrections involved in this experiment reveals no justification for revising the results presented.

The slight difference between the data presented here and that presented in a previous report of this experiment, <sup>16</sup> is due to a more complete analysis of the corrections made to the measurements.



MU-22795

Fig. 12. Total cross section for  $\pi^+$  - p as a function of the lab pion kinetic energy.



MU-22796

Fig. 13. Total cross section for  $\pi^- - p$  as a function of the lab pion kinetic energy.

Table II.

Summary of total cross section results					
$\pi^+ - p$			$\pi^- - p$		
$T_\pi$ (Mev)	$\sigma_T$ (mb)	$\Delta\sigma$ (mb)	$T_\pi$ (Mev)	$\sigma_T$ (mb)	$\Delta\sigma$ (mb)
457	29.44	1.63	452	33.03	0.69
506	24.14	2.11	503	36.01	0.61
529	22.87	1.80	554	41.86	0.81
651	17.95	1.34	598	46.20	0.84
749	21.58	0.65	652	41.67	0.78
805	24.98	0.74	705	40.23	1.05
861	27.10	0.50	727	40.66	0.58
890	25.79	0.39	755	42.09	0.88
906	27.04	0.80	800	44.71	0.76
952	26.98	0.66	852	52.74	0.63
998	28.90	0.58	873	55.97	0.71
1042	29.69	0.44	896	57.82	0.84
1100	31.80	0.44	920	56.95	0.86
1146	35.70	0.58	962	51.75	0.85
1183	36.76	0.41	993	46.66	0.64
1240	39.53	0.72	1022	42.37	0.62
1336	41.56	0.58	1045	41.17	0.59
1440	39.53	0.50	1100	37.18	0.61
1510	39.27	0.74	1150	36.55	0.71
			1195	35.84	1.22
			1240	35.22	0.60
			1300	35.72	0.93

Table II.(Continued)

---

Summary of total cross section results

---

$T_{\pi}$ (Mev)	$\pi^{-} - p$	
	$\sigma_T$ (mb)	$\Delta\sigma$ (mb)
1347	35.41	0.46
1416	34.51	0.54
1456	34.62	0.58
1520	33.81	0.73
1548	33.90	0.46
1584	33.40	0.46
1650	27.08	0.96

---

---

## V. DISCUSSION

### A. General

The distinctive features of the  $\pi^+$ -p total cross section in the energy range under consideration are as follows:

(a) The rapid decrease in the cross section as a function of energy between 450 Mev and 650 Mev. The cross section in this region is probably dominated by the tail of the "3-3 resonance," which has its peak at 200 Mev.

(b) A minimum in the cross section at about 650 Mev.

(c) The increase of the cross section to a "shoulder" centered at about 875 Mev.

(d) The continued increase to a maximum at about 1350 Mev, and subsequent decrease at higher energies to a constant value of 29.5 mb.<sup>13</sup>

The  $\pi^-$ -p cross section exhibits the following features:

(a) The rapid rise of the cross section to a maximum at 600 Mev.

(b) A minimum at approximately 700 Mev.

(c) Another, higher, maximum centered at 900 Mev.

(d) The decrease of the cross section to a broad plateau in the same region as the broad maximum in the  $\pi^+$ -p cross section.

In the following paragraphs we present the calculation of the cross section for the pure eigenstate of isotopic spin,  $T = 1/2$ , discuss possible assignments of the quantum numbers for the resonant states, and quote the results of a calculation of the real part of the forward scattering amplitude on the basis of dispersion relations.

### B. Cross Section for Pure $T = 1/2$ State

Under the assumption of charge independence, all the strong interactions between pions and nucleons can be described in terms of two eigenstates of isotopic spin. The pion has a isotopic spin of 1, and the nucleon, 1/2. The total I spin of the system consisting of one pion and one nucleon can thus be either 3/2 or 1/2. Charge independence states that, in isotopic spin space, the behavior of the system depends

only on the value of the total I spin, and is independent of its projection on the z axis. Thus, the I-spin part of the wave function of any of the six charge states in the pion-nucleon system may be written as a linear combination of the two eigenstates of I spin. If we develop the expressions for the total cross section we find, for the two cases under consideration in this experiment,

$$\sigma(\pi^+ - p) = \sigma(T = 3/2),$$

and

$$\sigma(\pi^- - p) = 2/3 \sigma(T = 1/2) + 1/3 \sigma(T = 3/2).$$

Solving these two equations for the pure  $T = 1/2$  state, we find

$$\sigma(T = 1/2) = 3/2 \sigma(\pi^- - p) - 1/2 \sigma(\pi^+ - p).$$

The results of a calculation of this cross section in the energy range under consideration are presented in Fig. 14.

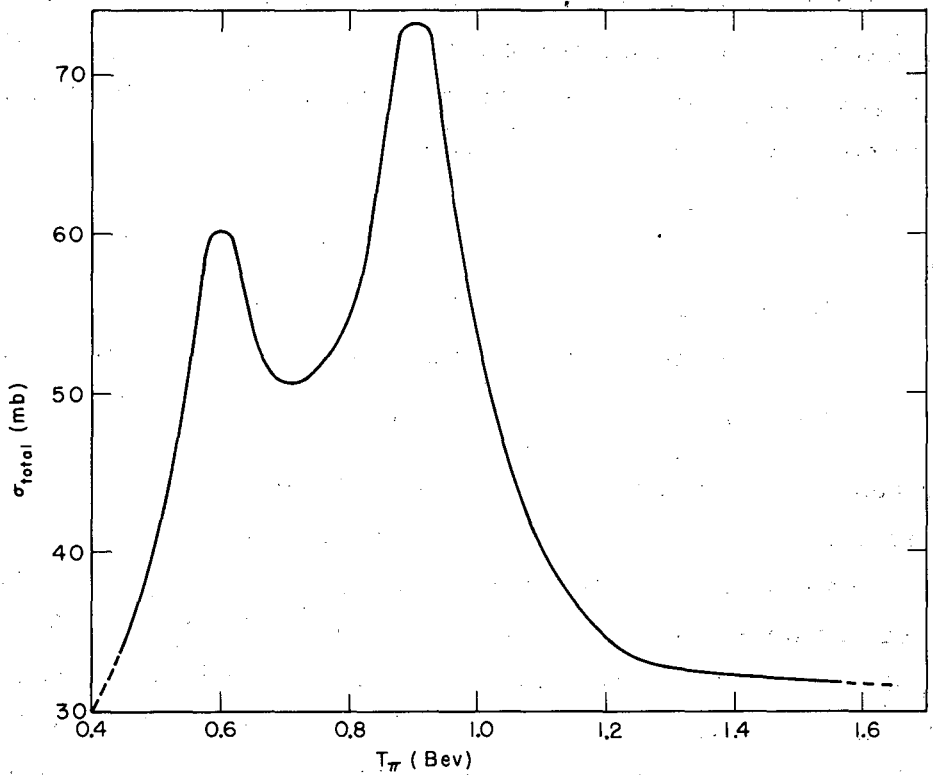
Qualitatively, the general features of the  $T = 1/2$  cross section are the same as the  $\pi^- - p$  cross section. The main difference is in the heights of the peaks, 60.2 mb at 600 Mev, and 73.2 mb at 900 Mev, and in the behavior of the flat portion of the curve above 1200 Mev. The  $T = 1/2$  cross section drops rapidly to a value below 32 mb, and is consistent with an asymptotic approach to the high-energy (4-Bev) value of about 30 mb.<sup>14</sup> Thus, the plateau observed in the  $\pi^- - p$  cross section can be ascribed to a contribution from the broad maximum in the pure  $T = 3/2$  state.

### C. Resonant States

If the expression for the total cross section is developed in terms of a partial-wave expansion of the scattering amplitudes for pion-nucleon scattering, we find that the maximum possible contribution from a given partial wave to the total cross section can be written (see Appendix B)

$$\sigma(\ell, J) = \pi\kappa^2 (2J + 1) (1 + b),$$

where  $\sigma(\ell, J)$  is the contribution to the total cross section from that



MU-22797

Fig. 14. Total cross section for the pure isotopic spin state,  $T = 1/2$ , as a function of lab pion kinetic energy.

partial wave having orbital angular momentum  $\ell$  and total angular momentum  $J$ ,  $\lambda$  is the deBroglie wave length of the pion in the center-of-mass system, and  $b$  is an inelastic scattering parameter which takes on values between 0 for pure diffraction scattering, and 1 for purely elastic scattering. We assume that we are dealing with the cross section for a pure isotopic spin state, and that the partial wave under consideration is in resonance, i. e., the phase shift  $\delta_{\ell, J}$  is 90 deg.

Let us examine the peaks in the  $T = 1/2$  isotopic spin state at 600 Mev and 900 Mev in the light of the above equation. Some qualitative observations are necessary to justify the procedure to be adopted. First, the widths (of the order of 150 Mev) and general shapes of these peaks are not unlike that of the 3-3 resonance in the  $T = 3/2$  cross section at 200 Mev. Since the behavior of the pion-nucleon cross section in the neighborhood of 200 Mev is quite adequately explained by a resonance in the state where  $\ell = 1$ ,  $J = 3/2$ , and  $T = 3/2$ , we are somewhat justified in assuming that the peaks at 600 Mev and 900 Mev are also due to resonant states. Secondly, there is an appreciable contribution to the cross section from partial waves other than the one in resonance. Goodwin indicates that, above 427 Mev, all partial waves up to  $F$  waves have a nonnegligible contribution to the angular distributions.<sup>15</sup> Thus, in analyzing the total cross section, it will be necessary to subtract a "nonresonant background" contribution from states other than the one in resonance.

If we assume that the nonresonant part of the cross section is about 30 mb--i. e., approximately equal to the asymptotic value of the total cross section at high energies--we can solve the above equation for  $b$ , trying several different values of the total angular momentum  $J$ . The results are shown in Table III.

At 600 Mev, the results are fairly clear, subject, of course, to the validity of the assumption about the nonresonant contribution. If, in fact, this is a resonant state, it probably has  $J = 3/2$ , with a fairly high amount of inelastic scattering. This conclusion is substantiated to some extent by data from a number of experiments collected

by Falk-Vairant and Valladas and presented at the 1960 Rochester Conference.<sup>17</sup> Measurements of the total elastic cross section (and, by subtraction, the total inelastic cross section) indicate the presence of a peak in both the elastic and inelastic cross sections at this energy. Qualitatively, this is the behavior to be expected from the value of  $b$  quoted in Table III for  $J = 3/2$ . The assignment of  $J = 3/2$  is also consistent with an analysis of the angular distribution for pion photoproduction,<sup>4</sup> which indicates that the proper assignment of quantum numbers for this resonance is  $l = 2$ , and  $J = 3/2$ .

At 900 Mev the results are somewhat ambiguous. With an assignment of 30 mb for the nonresonant contribution, three values of  $J$  fall in the acceptable range. Although not impossible, it seems unlikely that  $J$  is  $9/2$ . The indications of a peak in the inelastic cross section near 900 Mev<sup>17</sup> seem to rule out  $J = 5/2$  because of the value of  $b$ , which is very close to 1.0. However, analysis of photoproduction results,<sup>4</sup> although not conclusive, tends to favor the assignment of  $J = 5/2$ . These contradictory conclusions may be resolved if we assume a different value of the nonresonant contribution.

If the nonresonant contribution in the vicinity of 900 Mev has a behavior similar to that of the  $T = 3/2$  cross section near 1350 Mev, we would expect the value of this contribution to be about 40 mb. Under this assumption, the value of  $b$  for  $J = 5/2$  is more consistent with a substantial amount of inelastic scattering.

A recent experiment at Berkeley, measuring the elastic angular distribution for  $\pi^-$ -p scattering,<sup>18</sup> although not completely analyzed, is consistent with the suppositions of  $J = 3/2$  and  $J = 5/2$  for the two states, respectively, subject to the validity of the assumption that they are in resonance.

Table III

Values of inelastic coefficient for various assumptions about total angular momentum and nonresonant contribution						
T	$\sigma$ (total)	$\sigma$ (nonresonant)	$\sigma$ (resonant)	J	$\pi\lambda^2(2J+1)$	b
600	60.2	30	30.2	1/2	12.00	> 1
				3/2	24.1	0.251
				5/2	36.2	< 0
900	73.2	30	43.2	3/2	14.9	> 1
				5/2	22.4	0.93
				7/2	29.8	0.45
				9/2	37.3	0.16
				11/2	44.8	< 0
900	73.2	40	33.2	3/2	14.9	> 1
				5/2	22.4	0.48
				7/2	29.8	0.11
				9/2	37.3	< 0

#### D. Application of Dispersion Relations

The real part of the forward scattering amplitude for pion-proton scattering may be determined from the imaginary part by the dispersion relations.<sup>19</sup> The calculation involves integrals of the imaginary part over all energies. Since the imaginary part of the forward scattering amplitude is related to the total cross section by the optical theorem, the real part may be determined from the behavior of the total cross section. Explicitly,

$$\begin{aligned}
 D_{\pm}(k) = & 1/2 \left(1 \pm \frac{\omega}{\mu}\right) D_{+}(0) + 1/2 \left(1 \mp \frac{\omega}{\mu}\right) D_{-}(0) \\
 & + \frac{k^2}{4\pi^2} P \int_{\mu}^{\infty} \frac{d\omega'}{k'} \frac{\sigma_{\pm}(\omega')}{\omega' - \omega} \\
 & + \frac{k^2}{4\pi^2} \int_{\mu}^{\infty} \frac{d\omega'}{k'} \frac{\sigma_{\mp}(\omega')}{\omega' + \omega} \pm \frac{2f^2}{\mu^2} \frac{k^2}{\omega \mp \mu} \frac{1}{2M}
 \end{aligned}$$

where  $D_{\pm}(K)$  is the real part of the  $\pi^{\pm}$ -proton forward scattering amplitude at the pion laboratory-system wave number,  $k$ ;  $\omega$  is the total energy of the pion in the laboratory system;  $\mu$  is the pion mass;  $\sigma_{\pm}(\omega')$  is the total  $\pi^{\pm}$ -proton cross section at energy  $\omega'$ ;  $M$  is the nucleon mass. The units of  $k, \omega, \mu$ , and  $M$  are  $\text{cm}^{-1}$ .  $P$  means take the principal value of the integral. The coupling constant has the value  $f^2 = 0.08$ ; the starting values for the amplitudes are  $D_{+}(0) = -0.148 \times 10^{-13} \text{ cm}$  and  $D_{-}(0) = +0.106 \times 10^{-13} \text{ cm}$ .

Cronin has used the results of this experiment and others<sup>3, 13, 14, 21</sup> to perform this calculation. His results are contained in Ref. 20, and are shown in Fig. 15.

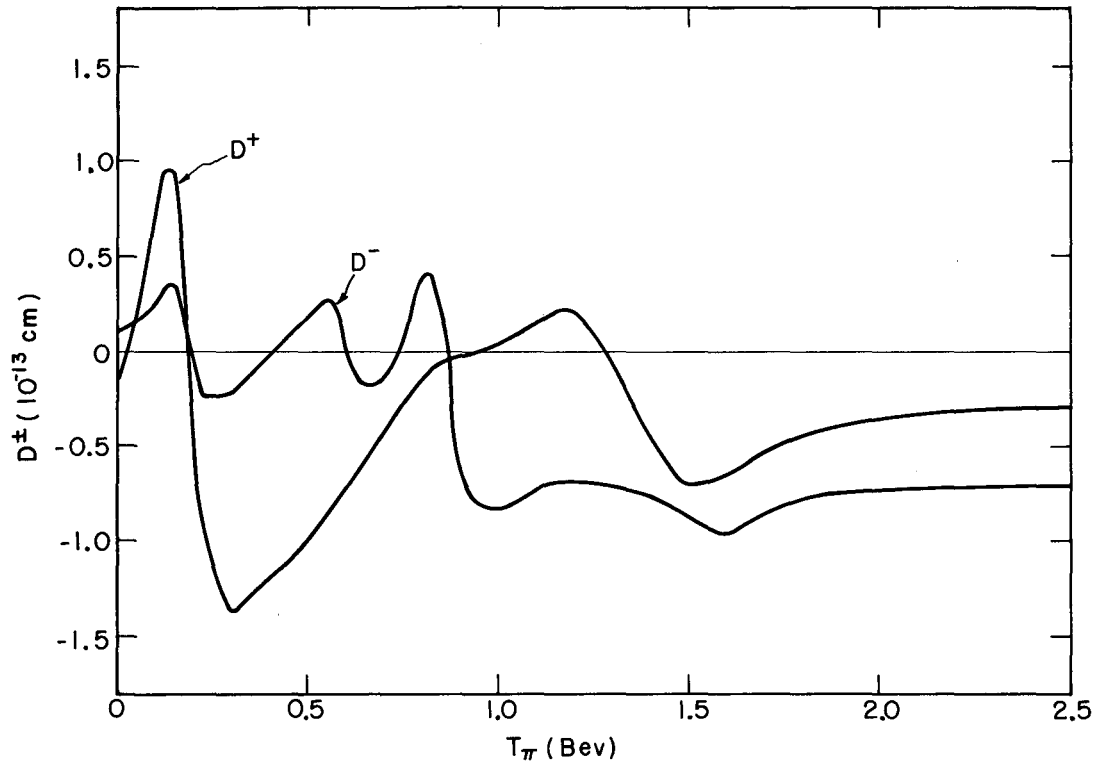
#### E. Comparison Between Scattering and Photoproduction

We wish to compare the results of pion scattering with the photoproduction reactions



At low energies it is expected that the influence of the strong final-state interaction in photoproduction will dominate the reaction and show a direct correspondence with the matching situations in pion scattering. As inelastic channels become more important at higher energies, this correspondence will be somewhat less evident; however, comparisons are still worth while.

A number of experiments dealing with Reaction (1) indicate the presence of a maximum in the cross section in the vicinity of 750-Mev energy(lab) of the gamma ray.<sup>22</sup> Other experiments<sup>23</sup> dealing with Reaction (2) show a maximum at about 700 Mev. If we assume that the maximum in the photoproduction cross section occurs at an energy where the total energy in the center-of-mass system is the same as that in the pion-proton scattering situation at 600 Mev, we would expect a maximum in photoproduction at 750 Mev. Thus there is good agreement between the scattering results and measurements



MU-22798

Fig. 15. Real part of the forward scattering amplitude for positive  $D^+$  and negative  $D^-$  pions on protons as a function of the lab pion kinetic energy.

of Reaction (1). The 50-Mev difference between the scattering results and Reaction (2) may be explained by a component of the photoproduction matrix which operates for charged meson photoproduction alone.<sup>4</sup> No estimate of the magnitude of the effect of this term is available.

## ACKNOWLEDGMENTS

The author owes a great debt of gratitude to Professor Burton J. Moyer for his patient guidance and gentlemanly example throughout this and other work. Special thanks are due to Professor A. C. Helmholz for his helpful advice on the academic aspects of graduate work.

Without the aid of Dr. Victor Perez-Mendez and Dr. Wilmot N. Hess, this experiment would have been immeasurably more difficult. Their suggestions during the design and execution of these measurements enabled the author to avoid many of the pitfalls into which the inexperienced experimenter falls.

In addition to the bonds of close friendship, the author owes much to Dr. Michael J. Longo. He has been an abundant source of suggestions and helpful criticism in all phases of this work.

The execution of an experiment of this magnitude requires the services of more than just a few men. For their diligent efforts and scientific skill during the rigors of a Bevatron experiment, many thanks are due to Mr. Paul McManigal, Mr. Jerome Helland, Mr. Barry Barish, Mr. Calvin Wood, Mr. Richard Eandi, Dr. John Atkinson, and Mr. Julius Solomon.

Grateful acknowledgment is given to the Bevatron staff and crew for their aid in setting up the apparatus and providing excellent running conditions for the experiment, and to the Computer Center staff for providing a complete and flexible method for data reduction.

Thanks are extended to the many members of the scientific and technical staff of the Lawrence Radiation Laboratory for a number of helpful discussions.

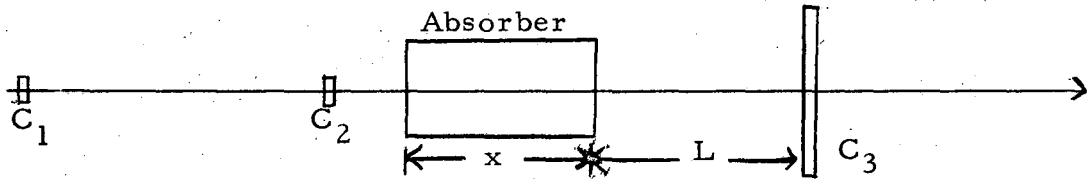
The value of the encouragement and enthusiasm supplied by Mr. and Mrs. Thomas J. Devlin, the author's parents, cannot be estimated. It is hoped that they will view this work as their own.

This work was done under the auspices of the U. S. Atomic Energy Commission.

APPENDICES

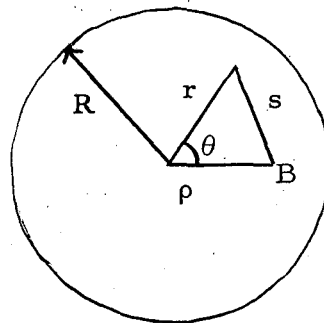
A. Derivation of Method for Coulomb Scattering Correction

Sternheimer<sup>11</sup> develops a method for making a Coulomb correction in the manner outlined below. We assume a simplified transmission experiment as shown in the figure below.



Counters  $C_1$  and  $C_2$  which monitor the beam incident on the absorber, and counter  $C_3$  monitors the transmitted beam. The length of the absorber is  $x$ , and the distance from absorber to the transmission counter is  $L$ . We assume that  $C_3$  is circular, and that the beam has cylindrical symmetry about the axis of  $C_3$ .

Consider a particle which in the absence of multiple scattering would traverse  $C_3$  at a distance  $\rho$  from the center of the counter, as shown below.



As a result of the scattering, there is a probability  $P$  (per unit area) that the particle will be found at a distance  $s$  from its position in the absence of scattering,  $B$ .  $P$  is given by

$$P = (1/\pi r_0^2) \exp(-s^2/r_0^2),$$

with

$$r_0 = \theta_s (x(L^2 + Lx + x^2/3))^{1/2},$$

where  $x$  and  $L$  are given above, and

$$\theta_s = (E_s / \beta c p) X_0^{-1/2},$$

where  $E_s = 21$  Mev,  $\beta c$  and  $P$  are the velocity and momentum of the particle, and  $X_0$  is the radiation length of the material.

Introducing polar coordinates at the center of  $C_3$ , we can write the probability as

$$P = (1 / \pi r_0^2) \exp \left[ -(r^2 + \rho^2 - 2r \rho \cos \theta) / r_0^2 \right]$$

Then the probability that the particle hits the counter is

$$f = \int_0^{2\pi} \int_0^R P r \, d\theta \, dr,$$

where  $R$  is the radius of  $C_3$ .

The explicit dependence on  $R$  can be removed by letting

$$r' = r/R, \quad \rho' = \rho/R, \quad \text{and} \quad r'_0 = r_0/R.$$

Sternheimer has numerically evaluated  $f$  in terms of  $r'_0$  and  $\rho'$ , and presents the results as a graph in his paper.

The function  $f$  gives the probability that a particle which, in the absence of scattering, would traverse  $C_3$  at a distance  $\rho$  from its center will not be scattered out of the counter. The dependence on the absorber and the geometry of the counter is contained in the parameter  $r_0$ .

With this information, and a knowledge of the dependence of the flux of particles,  $B(\rho)$ , as a function of distance from the center of  $C_3$ , we may calculate the fraction of the beam which is not scattered out of  $C_3$ .

This fraction,  $F$ , is given by

$$F = \int_0^{2\pi} \int_0^R B(\rho) f(\rho, r_0) \rho \, d\theta \, d\rho / \int_0^{2\pi} \int_0^R B(\rho) \rho \, d\theta \, d\rho.$$

B was measured during the experiment, and  $f$  is given by Sternheimer. These were numerically integrated to obtain the Coulomb correction.

### B. Partial-Wave Analysis

We present the familiar asymptotic expression for the wave function in a scattering situation at large distances from the scattering center:

$$u(r, \theta, \phi) = e^{ikz} + r^{-1} f(\theta, \phi) e^{ikr},$$

where the first and second terms are, respectively, the incident and scattered wave. In the pion-nucleon system, where spin must be considered, we must deal with the two scattering amplitudes for spin flip,  $f_\beta$ , and non spin flip,  $f_\alpha$ . If we expand these in eigenfunctions of the angular momentum states, we have

$$f_\alpha = k^{-1} \sum_l \left[ (l+1) a_{l+} + l a_{l-} \right] P_l^0(x),$$

and

$$e^{-i\phi} f_\beta = k^{-1} \sum_l \left[ a_{l-} - a_{l+} \right] P_l^1(x),$$

where  $a_{l+}$  and  $a_{l-}$  are the amplitudes for the  $J = l + 1/2$  and  $J = l - 1/2$  states respectively,  $x = \cos \theta$ , and  $P_l^m(x)$  is the associated Legendre polynomial.

The amplitudes may be written

$$a_{l\pm} = \left[ (\exp(2i\delta_{l\pm}) - 1) \right] / 2i.$$

when inelastic scattering is present, and the phase shift  $\delta$  is complex, we may write

$$a_{l\pm} = \left[ b_{l\pm} \exp(2ia_{l\pm}) - 1 \right] / 2i,$$

where  $a$  is the real part of the phase shift, and

$$b_{l\pm} = \exp \left[ -2\beta_{l\pm} \right],$$

REFERENCES

1. H. Bethe and F. deHoffman, Mesons and Fields, Vol. 2, (Row Peterson, Evanston, Ill., 1955). This reference contains a summary of work done before 1955.
2. R. Cool, O. Piccioni, and D. Clark, Phys. Rev. 103, 1082 (1956).
3. H. C. Burrowes, D. O. Caldwell, D. H. Frisch, D. A. Hill, D. M. Ritson, R. A. Schluter, and M. A. Wahlig, Phys. Rev. Letters 2, 119 (1959).
4. Ronald F. Peierls, Phys. Rev. 118, 325 (1960).
5. Duane B. Newhart, Victor Perez-Mendez, and William H. Pope, Liquid-Hydrogen Target, Lawrence Radiation Laboratory Report UCRL-8857, August 1959 (unpublished).
6. John H. Atkinson and Victor Perez-Mendez, Rev. Sci. Instr. 30, 865 (1959).
7. William A. Wenzel, Millimicrosecond Coincidence Circuit for High-Speed Counting, Radiation Laboratory Report UCRL-8000, Oct. 2 1957 (unpublished).
8. David F. Swift and Victor Perez-Mendez, Millimicrosecond Discriminator, Lawrence Radiation Laboratory Report UCRL-8569, December 1958 (unpublished).
9. Lawrence Radiation Laboratory Counting Handbook, Lawrence Radiation Laboratory Report UCRL-3307-Rev., Jan. 1959 (unpublished).
10. John H. Atkinson, Jr. and Beverly Hill Willis, High-Energy Particle Data, Vol. 2, University of California Radiation Laboratory Report UCRL-2426-Rev. June 1957 (unpublished).
11. R. M. Sternheimer, Rev. Sci. Instr. 25, 1070 (1954).
12. Walter H. Barkas and Arthur H. Rosenfeld, Data for Elementary-Particle Physics, University of California Radiation Laboratory Report UCRL-8030, March 20, 1958 (unpublished).
13. M. J. Longo, J. A. Helland, W. N. Hess, B. J. Moyer, and V. Perez-Mendez, Phys. Rev. Letters 3, 568 (1959).

14. F. Wikner, Nuclear Cross Sections for 4.2-Bev Negative Pions, University of California Radiation Laboratory Report UCRL-3639, January 10, 1957 (unpublished).
15. Lester K. Goodwin, The Elastic Scattering of Negative Pions by Protons at 230, 290, 370, and 427 Mev (Ph. D. Thesis), Lawrence Radiation Laboratory Report UCRL-9119, April 7, 1960 (unpublished).
16. T. J. Devlin, B. C. Barish, W. N. Hess, V. Perez-Mendez, and J. Solomon, Phys. Rev. Letters 4, 242 (1960).
17. P. Falk-Vairant and G. Valladas, Results in Pion-Proton Scattering Near the Higher Resonances, in Proceedings of the 1960 Annual International Conference on High-Energy Physics at Rochester (University of Rochester; Interscience, New York, 1960), p. 38.
18. C. D. Wood, T. J. Devlin, J. A. Helland, M. J. Longo, B. J. Moyer, and V. Perez-Mendez, Bull. Am. Phys. Soc. 5, 509 (1960).
19. M. L. Goldberger, Phys. Rev. 99, 979 (1955); R. Karplus and M. A. Ruderman, Phys. Rev. 98, 771 (1955); M. L. Goldberger, H. Miyazawa, and R. Oehme, Phys. Rev. 99, 986 (1955); H. L. Anderson, W. C. Davidon, U. E. Kruse, Phys. Rev. 100, 339 (1955).
20. J. W. Cronin, Phys. Rev. 118, 824 (1960).
21. J. C. Brisson, J. Detoef, P. Falk-Vairant, L. van Rossum, G. Valladas, and L. C. L. Yuan, Phys. Rev. Letters 3, 561 (1959).
22. J. W. DeWire, H. E. Jackson, and R. Littauer, Phys. Rev. 110, 1208 (1958); P. C. Stein and K. C. Rogers, Phys. Rev. 110, 1209 (1958); J. I. Vette, Phys. Rev. 111, 622 (1958); K. Berkelman and J. A. Waggoner, Phys. Rev. 117, 1364 (1960).
23. M. Heinberg, W. M. McClelland, F. Turkot, W. M. Woodward, R. R. Wilson and D. M. Zipoy, Phys. Rev. 110, 1211 (1958); F. P. Dixon and R. L. Walker, Phys. Rev. Letters 1, 142 (1958); L. Hand and C. Schaerf, Phys. Rev. Letters 6, 229 (1961).

This report was prepared as an account of Government sponsored work. Neither the United States, nor the Commission, nor any person acting on behalf of the Commission:

- A. Makes any warranty or representation, expressed or implied, with respect to the accuracy, completeness, or usefulness of the information contained in this report, or that the use of any information, apparatus, method, or process disclosed in this report may not infringe privately owned rights; or
- B. Assumes any liabilities with respect to the use of, or for damages resulting from the use of any information, apparatus, method, or process disclosed in this report.

As used in the above, "person acting on behalf of the Commission" includes any employee or contractor of the Commission, or employee of such contractor, to the extent that such employee or contractor of the Commission, or employee of such contractor prepares, disseminates, or provides access to, any information pursuant to his employment or contract with the Commission, or his employment with such contractor.